Material Interface in the Finite-Difference Modeling: A Fundamental View

Peter Moczo*[1], Jozef Kristek[1], Miriam Kristekova[2], Jaroslav Valovcan[1], Martin Galis[1], and David Gregor[3]

ABSTRACT

By analyzing the equations of motion and constitutive relations in the wavenumber domain, we gain important insight into attributes determining the accuracy of finite-difference (FD) schemes. We present heterogeneous formulations of the equations of motion and constitutive relations for four configurations of a wavefield in an elastic isotropic medium. We Fourier-transform the entire equations to the wavenumber domain. Subsequently, we apply the band-limited inverse Fourier transform back to the space domain. We analyze consequences of spatial discretization and wavenumber band limitation. The heterogeneity of the medium and the Nyquist-wavenumber band limitation of the entire equations has important implications for an FD modeling: The grid representation of the heterogeneous medium must be limited by the Nyquist wavenumber. The wavenumber band limitation replaces spatial derivatives both in the homogeneous medium and across a material interface by continuous spatial convolutions. The latter means that the wavenumber band limitation removes discontinuities of the spatial derivatives of the particle velocity and stress at the material interface. This allows to apply proper FD operators across material interfaces. A wavenumber band-limited heterogeneous formulation of the equations of motion and constitutive relations is the general condition for a heterogeneous FD scheme.

KEY POINTS

- We address fundamentals of the finite-difference (FD) modeling of seismic wave propagation and earthquake motion.
- Implications of heterogeneity of medium and spatial discretization for FD schemes are found.
- Grid representation of a heterogeneous medium must be limited by the Nyquist wavenumber.

INTRODUCTION

Topics of the finite-difference (FD) method

The FD method in present-day seismology is a global name for a large family of numerical-modeling methodologies. They all are based on one unifying concept: approximating equations, boundary conditions and initial conditions by an FD scheme. A complete FD methodology must comprise a time–space grid; schemes for updating wavefield at interior grid points, points at and near the Earth's free surface, and points at and near the other borders of the grid; a rheological model of the medium; a discrete representation of smooth and discontinuous material heterogeneity; a discrete representation of a wavefield source. Individual FD methodologies used in seismology differ in one or several of these constituents. They rarely comprise all the state-of-the-art ingredients.

The most significant development in FD methodology in recent years has been focused on the optimal FD approximations of the spatial derivatives. The goal of development is to find FD approximations with (1) the same high-order accuracy in space and time, in all propagation directions and in a wide range of wavenumbers, and (2) optimal balance between increasing order of accuracy and computational demands. For recent reviews, we refer to Zhou *et al.* (2021) and Moczo *et al.* (2021).

The task of finding the best FD approximation is definitively far from being trivial and, thus, understandably, most of the authors have not addressed the other persisting and pertinent aspect of FD schemes—implementation of internal material interfaces.

The most important approaches to represent a material interface in an FD grid until 2013 are comprehensively presented by Moczo *et al.* (2014) and analyzed by Vishnevsky *et al.* (2014). Here, we will mention the important contributions developed afterward.

1. Faculty of Mathematics, Physics and Informatics, Comenius University in Bratislava, Bratislava, Slovakia, https://orcid.org/0000-0001-5276-9311 (PM); https://orcid.org/0000-0002-2332-541X (JK); https://orcid.org/0000-0002-7728-2064 (JV); https://orcid.org/0000-0002-5375-7061 (MG); 2. Earth Science Institute, Slovak Academy of Sciences, Bratislava, Slovakia, https://orcid.org/0000-0001-9017-5952 (MK); 3. University of Grenoble Alpes, University of Savoie Mont Blanc, CNRS, IRD, University of Gustave Eiffel, ISTerre, Grenoble, France, https://orcid.org/0000-0003-0291-4044 (DG)

*Corresponding author: moczo@fmph.uniba.sk

Cite this article as Moczo, P., J. Kristek, M. Kristekova, J. Valovcan, M. Galis, and D. Gregor (2022). Material Interface in the Finite-Difference Modeling: A Fundamental View, *Bull. Seismol. Soc. Am.* **113**, 281–296, doi: 10.1785/0120220133

Recent advances in representation of material interfaces

Mittet (2017) represented a sharp (high impedance contrast) material interface in elastic media using a Heaviside step function in the space domain, transformed the representation to the wavenumber domain, and eventually returned to the space domain using a band-limited inverse Fourier transform. The maximum wavenumber corresponds to the one allowed by a spatial grid. Mittet (2017) also suggested an alternative approach: a fine-grid model is created first, and then it is low-pass filtered to remove wavenumbers inappropriate for the coarser grid used for the FD simulation. The fine grid is then sampled at the required coordinates for the coarse grid. Mittet (2021a,b) elaborated clever detailed analyses of accuracy of his approach, explained the cause of some typical numerical errors appearing in pseudospectral and FD simulations in heterogeneous media, and investigated the implementation of small-scale heterogeneities. Mittet (2021a,b) demonstrated a sub-cell resolution of his implementation.

Moczo *et al.* (2014, 2019), Kristek *et al.* (2017, 2019), and Gregor *et al.* (2021, 2022) developed orthorhombic representations of strongly heterogeneous elastic, viscoelastic, and poroelastic media with material interfaces. Their main idea was to best represent smooth and discontinuous material heterogeneity in the FD modeling using the standard staggered-grid scheme (fourth-order accurate in space, second-order accurate in time). All schemes keep computational efficiency of the corresponding velocity–stress or velocity–pressure–stress staggered grid schemes for smoothly and weakly heterogeneous media while having a sub-cell resolution capability. The viscoelastic medium has rheology of the generalized Maxwell body (equivalent to the generalized Zener body). The poroelastic medium may have zero resistive friction or nonzero resistive friction or Johnson-Koplik-Dashen frequency-dependent permeability and resistive friction. All FD schemes are capable of sub-cell resolution.

Mittet (2017) observed that there are cases in seismic exploration in which an accurate description of interface is important (the seabed being a good example). Moczo *et al.* (2018) pointed out the need for, and importance of geometrically and rheologically complex models in identifying key structural parameters and key characteristics of earthquake ground motion.

Jiang and Zhang (2021) developed a tilted transversely isotropic equivalent medium parameterization method for representing tilted elastic material interfaces in higher order FD schemes on a coarse Lebedev grid. The authors report that their method has a sub-cell resolution capability. For the horizontal interface, the equivalent elasticity matrix is the same as that of the orthorhombic representation (Kristek *et al.*, 2017). If the material interface passes through the grid cell at an arbitrary angle, the Bond transformation is applied for obtaining the tilted transversely isotropic equivalent medium.

Koene *et al.* (2022) tested and compared several approaches to represent tilted (dipping) material interfaces: sampling at coarse resolution (a local pointwise representation of any material heterogeneity), an anti-aliased step function and low-pass filtering of the high-resolution oversampled grid model (the two mentioned Mittet's approaches), an equivalent medium with Schoenberg–Muir calculus (Schoenberg and Muir, 1989; Muir *et al.*, 1992), and an equivalent medium with orthorhombic averaging (Moczo *et al.*, 2014; Kristek *et al.*, 2017), which coincides with the Schoenberg–Muir approach for an interface parallel with a grid plane. Based on their method of comparison, they conclude that the Schoenberg–Muir approach is an efficient method to minimize errors in elastic simulations with inclined interfaces in 2D problems.

Specific aspects

There are several interesting aspects of representing and implementing material interfaces in FD schemes. We mention them here because they are very relevant and motivating for this article.

- The Heaviside step function was used for representing a material interface by Zahradník and Priolo (1995). They used it in their theoretical analysis to show that the 2D displacement formulation of the equation of motion can be considered a heterogeneous formulation of the equation of motion which can account for presence of the material interface without explicit use of the boundary conditions if material heterogeneity is properly implemented in an FD scheme. Zahradník and Priolo, however, did not directly use the Heaviside step function to implement the material interface in their FD scheme. Neither did they apply the grid-imposed wavenumber band limitation. Moczo (1998) pointed out the idea of Zahradník and Priolo (1995) but did not use the Heaviside step function either to represent the material interface.
- Mittet (2017) observed that a simple product of a material coefficient and a wavefield variable in the spatial domain corresponds to a convolution in the wavenumber domain.
- It is well known that spatial derivatives of wavefield variables are discontinuous at the material interface. In the heterogeneous FD schemes, FD spatial operators are applied in all interior grid points to calculate spatial derivatives of the wavefield variables. We are not aware of any paper explaining whether it is possible or not across an interface.
- We in our previous papers and, as far as we know, other numerical modelers simply applied FD spatial operators to calculate spatial derivatives of the wavefield variables across the material interface without explaining whether it is possible or not.
- It is commonly assumed that using the higher order spatial FD operators improves accuracy, but we are not aware of any explanation why this should be so if the long-stencil spatial operator is applied across the material interface.
- Mora (1986), Igel *et al.* (1995), and Fichtner (2011) replaced spatial derivatives by the wavenumber band-limited discrete

operators—they correctly applied the wavenumber limit imposed by the spatial grid. They, however, did not address the presence of a material interface.
- To the best of our knowledge, the Fourier transform to the wavenumber domain and the subsequent band-limited inverse Fourier transform back to the space domain have not been applied to the entire equations of motion and constitutive relations to examine the fundamental implications for FD approximations of the equations. The wavenumber-domain view on the entire equations is the key novel aspect of our approach.

Structure of this article

In this article, we address the following topics:

1. elemental consideration on implementation of a material interface in an FD grid;
2. 1D problem in an unbounded homogeneous elastic medium: time–space domain view and frequency–wavenumber view;
3. 1D, 2D *SH*, and 3D problem in a model of two homogeneous elastic half-spaces: time–space domain view and frequency–wavenumber view; and
4. implications for FD modeling.

Let us point out one aspect. We restrict our analysis to the simplest case of a planar material interface perpendicular to a coordinate axis. We do this for two basic reasons: (a) It is important to investigate the implications of the presence of a material interface (the simplest sharp spatial heterogeneity) in the simplest possible grid position (perpendicular to a coordinate axis) for the FD modeling. (b) A planar interface in a general orientation and a nonplanar interface bring such additional complexity to the problem that they require special approximate approaches. At the same time, they do not cancel or reduce the importance of the findings based on the analysis of the interface considered in this study.

ELEMENTAL CONSIDERATION ON A MATERIAL INTERFACE IN AN FD GRID

For simplicity and essential view, consider a 1D problem of two homogeneous half-spaces. Next, consider, for example, a velocity–stress formulation of the equation of motion and constitutive law. From now on, for brevity, they will be referred to as V_S equations.

We want to solve the problem using a heterogeneous FD scheme, that is, one and the same scheme for any interior grid point no matter what the position of the grid point with respect to the material interface is.

The heterogeneous FD scheme must solve such V_S equations that are valid for any point (any spatial position, not a grid point here) of the medium. We may call the corresponding V_S equations a heterogeneous formulation of the V_S equations. It must have the same form for a point away of the material interface and a point directly at the material interface. Obviously, it must account for the boundary conditions at the material interface. The implementation of the boundary conditions can be achieved by considering equations for both half-spaces, explicit accounting for continuity of continuous wavefield variables, and accompanying averaging of discontinuous wavefield variables and material parameters.

The implementation of the boundary conditions determines a structure of the heterogeneous formulation. The heterogeneous formulation corresponds to principles of averaging presented by Backus (1962).

There is another equally important aspect of constructing an FD scheme. The scheme is constructed on a spatial grid. Assume a uniform spatial grid with a grid spacing h. Considering the Nyquist sampling limit, the minimum wavelength that can be "seen" (supported or propagated) by the grid is $\lambda_{\min} = 2h$. The corresponding maximum spatial frequency, the Nyquist wavenumber, is $k_N = 2\pi/\lambda_{\min} = \pi/h$. Consequently, an FD discretization of the heterogeneous formulation of the V_S equations should account for the maximum admissible wavenumber.

This can be achieved in three steps: (a) Fourier transformation of the time–space heterogeneous formulation into the time–wavenumber domain, (b) wavenumber $k \in \langle -k_N, k_N \rangle$ band-limited inverse Fourier transformation back to the time–space domain, and (c) FD discretization of the wavenumber band-limited heterogeneous formulation.

We can see that as soon as we assume a spatial grid for constructing a heterogeneous FD scheme, we immediately involve two interconnected aspects of construction: a heterogeneous formulation with its averaging structure and wavenumber band limitation.

Thus, if we want to solve V_S equations by a heterogeneous FD scheme, we need (a) a heterogeneous formulation of the V_S equations and (b) wavenumber band limitation. The wavenumber band limitation must be applied to the heterogeneous formulation.

In the following sections, we present detailed analyses of four canonical problems to identify the basic aspects of the FD discretization: 1D problem in an unbounded medium, 1D problem in two homogeneous half-spaces, 2D *SH* problem in two homogeneous half-spaces, and eventually 3D problem in two homogeneous half-spaces. The unbounded medium is analyzed to obtain basic consequences of the wavenumber band limitation.

1D PROBLEM IN AN UNBOUNDED HOMOGENEOUS MEDIUM

Time–space domain view

Wave propagation in an unbounded homogeneous elastic medium can be described by the V_S equations:

$$\rho \frac{\partial v(z,t)}{\partial t} = \frac{\partial \sigma(z,t)}{\partial z}, \; C \frac{\partial \sigma(z,t)}{\partial t} = \frac{\partial v(z,t)}{\partial z}, \tag{1}$$

in which ρ and C are density and compliance, $v(z,t)$ and $\sigma(z,t)$ are the particle velocity and stress, and z and t are the spatial coordinate and time, respectively.

Assume an FD scheme solving these equations. A stability analysis of the scheme yields a stability condition for a time step $\Delta t(c,h)$, in which $c = 1/\sqrt{\rho C}$ is the wave speed and h is a grid spacing. A dispersion analysis yields a dispersion error $\varepsilon(N_\lambda, p_{\Delta t})$ as a function of the number of grid spacings N_λ per wavelength λ for a chosen value $p_{\Delta t}$ of a fraction of the maximum possible Δt. A model of medium together with the maximum angular frequency ω_{max} of the wavefield imply a minimum wavelength $\lambda_{min} = 2\pi c/\omega_{max}$. A choice of an admissible value of the error ε, based on an appropriate criterion, implies $N_{\lambda_{\min}}$ and, consequently, values of the grid spacing h and time step Δt.

Frequency–wavenumber domain view

Consider the following definitions of the Fourier and inverse Fourier transforms:

$$\begin{aligned}\tilde{\hat{\varphi}}(k,\omega) &= \mathcal{F}_{t\to\omega,z\to k}\{\varphi(z,t)\}\\ &\equiv \int_{-\infty}^{\infty}\left[\int_{-\infty}^{\infty}\varphi(z,t)\exp(-i\omega t)dt\right]\exp(ikz)dz\\ &\equiv \int_{-\infty}^{\infty}[\hat{\varphi}(z,\omega)]\exp(ikz)dz\\ \varphi(z,t) &= \mathcal{F}^{-1}_{\omega\to t,k\to z}\{\tilde{\hat{\varphi}}(k,\omega)\}\\ &\equiv \frac{1}{2\pi}\int_{-\infty}^{\infty}\left[\frac{1}{2\pi}\int_{-\infty}^{\infty}\tilde{\hat{\varphi}}(k,\omega)\exp(i\omega t)d\omega\right]\exp(-ikz)dk\\ &\equiv \frac{1}{2\pi}\int_{-\infty}^{\infty}[\tilde{\varphi}(k,t)]\exp(-ikz)dk. \end{aligned} \quad (2)$$

Here, k and ω mean wavenumber and angular frequency, respectively. Application of $\mathcal{F}_{t\to\omega,z\to k}$ to equation (1) gives,

$$-\omega\rho\tilde{\hat{v}}(k,\omega) = k\tilde{\hat{\sigma}}(k,\omega), -\omega C\tilde{\hat{\sigma}}(k,\omega) = k\tilde{\hat{v}}(k,\omega). \quad (3)$$

We consider a continuum (that is, not a grid of discrete points or a mesh of elements). However, having in mind an FD scheme solving equation (1), we will look at the equations from the perspective of the FD discretization. A discretization necessarily implies limitations in the frequency and wavenumber domains.

We can always choose a source-time function with spectrum limited to $\omega < \omega_{\max}$. Therefore, in our analysis we may restrict to $\mathcal{F}_{z\to k}$ and consider V_S equations in the following form instead of equation (3):

$$\rho\frac{\partial\tilde{v}(k,t)}{\partial t} = -ik\tilde{\sigma}(k,t), C\frac{\partial\tilde{\sigma}(k,t)}{\partial t} = -ik\tilde{v}(k,t). \quad (4)$$

Now, we need an elementary but important consideration. Assume $v = 0$ and $\sigma = 0$ at $t = 0$, that is, prior activation of the wavefield source. Then the source limits wavefield to frequencies $\omega < \omega_{\max}$. This and the wave speed c imply the minimum wavelength $\lambda_{\min} = 2\pi c/\omega_{\max}$ and thus the maximum wavenumber $k_N = 2\pi/\lambda_{\min}$. Next, consider a spatial discretization. The Nyquist spatial sampling admits the maximum grid spacing $h = \lambda_{\min}/2$ and thus $k_N = \pi/h$. Consequently, the wavenumber spectrum of the simulated wavefield is all the time(!) limited to $k \in \langle -k_N, k_N\rangle$.

There are two immediate consequences:

1. We have to apply a band-limited inverse Fourier transform to equation (4):

$$\begin{aligned}\mathcal{F}^{-1}_{k\to z}|^{k_N}_{-k_N}\left\{\rho\frac{\partial\tilde{v}(k,t)}{\partial t}\right\} &= \mathcal{F}^{-1}_{k\to z}|^{k_N}_{-k_N}\{-ik\tilde{\sigma}(k,t)\}\\ \mathcal{F}^{-1}_{k\to z}|^{k_N}_{-k_N}\left\{C\frac{\partial\tilde{\sigma}(k,t)}{\partial t}\right\} &= \mathcal{F}^{-1}_{k\to z}|^{k_N}_{-k_N}\{-ik\tilde{v}(k,t)\}. \end{aligned} \quad (5)$$

2. For the left sides of equation (5), we can write,

$$\begin{aligned}\mathcal{F}^{-1}_{k\to z}|^{k_N}_{-k_N}\left\{\rho\frac{\partial\tilde{v}(k,t)}{\partial t}\right\} &= \rho\mathcal{F}^{-1}_{k\to z}|^{\infty}_{-\infty}\left\{\frac{\partial\tilde{v}(k,t)}{\partial t}\right\} = \rho\frac{\partial v(z,t)}{\partial t}\\ \mathcal{F}^{-1}_{k\to z}|^{k_N}_{-k_N}\left\{C\frac{\partial\tilde{\sigma}(k,t)}{\partial t}\right\} &= C\mathcal{F}^{-1}_{k\to z}|^{\infty}_{-\infty}\left\{\frac{\partial\tilde{\sigma}(k,t)}{\partial t}\right\} = C\frac{\partial\sigma(z,t)}{\partial t}. \end{aligned} \quad (6)$$

Consider the right sides of equation (5). The bands-limited inverse Fourier transform is to be applied to the spectral product of $-ik$ and $\tilde{\sigma}(k,t)$ or $\tilde{v}(k,t)$. We know from the convolution theorem that an inverse Fourier transform of a product of two spectra is equal to a convolution of inverse Fourier transforms of individual spectra. The question is whether this is valid also in the range of $k \in \langle -k_N, k_N\rangle$. In Appendix A, we show that for $\tilde{\varphi}_1(k)$ and $\tilde{\varphi}_2(k)$ equal to zero outside $\langle -k_{\max}, k_{\max}\rangle$,

$$\begin{aligned}&\mathcal{F}^{-1}_{k\to z}|^{k_{\max}}_{-k_{\max}}\{\tilde{\varphi}_1(k,t)\tilde{\varphi}_2(k,t)\} = \mathcal{F}^{-1}_{k\to z}|^{k_{\max}}_{-k_{\max}}\{\tilde{\varphi}_1(k,t)\}*^z\\ &\mathcal{F}^{-1}_{z\to k}|^{k_{\max}}_{-k_{\max}}\{\tilde{\varphi}_2(k,t)\}. \end{aligned} \quad (7)$$

Here, z above * indicates convolution in the spatial domain. Since

$$\mathcal{F}^{-1}_{k\to z}|^{k_N}_{-k_N}\{-ik\} = \frac{1}{hz}\cos\left(\frac{\pi z}{h}\right) - \frac{1}{\pi z^2}\sin\left(\frac{\pi z}{h}\right), \quad (8)$$

and, based on the consideration preceding equations (5) and (6),

$$\mathcal{F}^{-1}_{k\to z}|^{k_N}_{-k_N}\{\tilde{\varphi}(k,t)\} = \varphi(z,t); \varphi \in \{\sigma, v\}, \quad (9)$$

the application of the $k \in \langle -k_N, k_N\rangle$ band-limited inverse Fourier transform to equation (4) yields,

$$\begin{aligned}\rho\frac{\partial v(z,t)}{\partial t} &= \left[\frac{1}{hz}\cos\left(\frac{\pi z}{h}\right) - \frac{1}{\pi z^2}\sin\left(\frac{\pi z}{h}\right)\right]*^z\sigma(z,t)\\ C\frac{\partial\sigma(z,t)}{\partial t} &= \left[\frac{1}{hz}\cos\left(\frac{\pi z}{h}\right) - \frac{1}{\pi z^2}\sin\left(\frac{\pi z}{h}\right)\right]*^z v(z,t). \end{aligned} \quad (10)$$

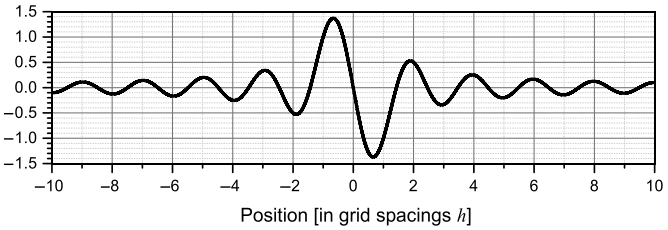

Figure 1. Illustration of the spatial function in convolutions in equation (10).

This equation is the $k \in \langle -k_N, k_N \rangle$ band-limited version of the original equation (1). The function in convolution (derivative of function sinc) is illustrated in Figure 1.

Let us observe that there is an alternative way of reaching equation (10). The right sides of equation (5) can be treated as follows. Because $\tilde{\sigma}(k, t)$ and $\tilde{v}(k, t)$ are band limited within $\langle -k_N, k_N \rangle$, as explained earlier, it is possible to replace the band-limited integration by the ordinary inverse Fourier transform and ik by $ik\Pi(k/k_N)$, in which Π is the standard centered (unit-width) boxcar function. The inverse Fourier transform of $ik\Pi(k/k_N)$ is the derivative of a sinc function.

The first lesson from the wavenumber-domain view

Assuming the maximum wavefield frequency $\omega_{\max}$, due to source spectrum, and the Nyquist wavenumber $k_N = \pi/h$, due to grid spacing h, we have transformed equation (1) to (10). Equations are valid for unlimited ranges of time, space, frequency, and wavenumber in an unbounded homogeneous elastic medium. Equation (1) is $k \in \langle -k_N, k_N \rangle$ band-limited in the wavenumber domain. The spatial derivatives of the particle velocity and stress are replaced by continuous spatial convolution integrals for $z \in (-\infty, \infty)$.

Because the unbounded computational domain must be replaced by a finite spatial grid, the continuous spatial convolution integrals for $z \in (-\infty, \infty)$ must be approximated by discrete convolution sums within a finite range of z.

The most important aspect is that the FD-simulated wavefield in a grid model of an unbounded homogeneous medium can be, in principle, accurate up to the Nyquist wavenumber k_N.

1D PROBLEM IN TWO HOMOGENEOUS HALF-SPACES

Consider a model of two homogeneous half-spaces, labeled − and + for $z < z_{\mathrm{MI}}$ and $z > z_{\mathrm{MI}}$, respectively, with a welded material interface at $z = z_{\mathrm{MI}}$. Material parameters are discontinuous at the material interface. The boundary conditions at the material interface are continuity of the particle velocity v and continuity of stress σ. Spatial derivatives $\partial v/\partial z$ and $\partial \sigma/\partial z$ are discontinuous at the material interface.

Equations in the time–space domain

Velocity–stress equations inside half-spaces. With an obvious abbreviated notation, we may write the V_S equations in the half-spaces as,

$$\rho^- \frac{\partial v(z,t)}{\partial t} = \frac{\partial \sigma(z,t)^-}{\partial z}, \rho^+ \frac{\partial v(z,t)}{\partial t} = \frac{\partial \sigma(z,t)^+}{\partial z}, \quad (11)$$

$$C^- \frac{\partial \sigma(z,t)}{\partial t} = \frac{\partial v(z,t)^-}{\partial z}, C^+ \frac{\partial \sigma(z,t)}{\partial t} = \frac{\partial v(z,t)^+}{\partial z}. \quad (12)$$

Velocity–stress equations at the material interface. To find V_S equations at the material interface, we need to combine equations (11) and (12), and the boundary conditions at the material interface. In the equations of motion (equation 11), we account for the continuity of temporal derivatives of the particle velocity and arithmetically average discontinuous spatial derivatives of stress. This implies that also densities are arithmetically averaged at the material interface. In the constitutive equation (12), we account for the continuity of temporal derivatives of stress and arithmetically average discontinuous spatial derivatives of the particle velocity. This implies that also compliances are arithmetically averaged at the material interface. Thus, we have,

$$\langle \rho \rangle^z \frac{\partial v}{\partial t} = \left\langle \frac{\partial \sigma}{\partial z} \right\rangle^z, \langle C \rangle^z \frac{\partial \sigma}{\partial t} = \left\langle \frac{\partial v}{\partial z} \right\rangle^z. \quad (13)$$

Equations (1) are
Equations (10) are

Here, $\langle\rangle^z$ indicates the arithmetic averaging at the material interface:

$$\left\langle \frac{\partial \varphi}{\partial z} \right\rangle^z := \frac{1}{2}\left(\left.\frac{\partial \varphi}{\partial z}\right|_{z=z_{\mathrm{MI}}^-} + \left.\frac{\partial \varphi}{\partial z}\right|_{z=z_{\mathrm{MI}}^+} \right) = \left.\frac{\partial \varphi}{\partial z}\right|_{z=z_{\mathrm{MI}}}; \varphi \in \{v, \sigma\}, \quad (14)$$

$$\langle p \rangle^z = \frac{1}{2}(p^- + p^+) = p|_{z=z_{\mathrm{MI}}}; p \in \{\rho, C\}. \quad (15)$$

Let us underline: though equation (13) is valid at the material interface, importantly, apart from the averaging, they have the same forms as the equations inside the half-spaces.

Velocity–stress equations for the entire model: A heterogeneous formulation. Equation (13) can be also considered equations valid for the entire model. This is because (a) at any spatial position inside the half-spaces the averages give correct local values of the material parameters and field variables, and (b) at the material interface they properly average both the material parameters and spatial derivatives.

Equation (13) can be specified for the entire model of the two homogeneous half-spaces as,

$$[\rho^{-}H(z_{\mathrm{MI}}-z)+\rho^{+}H(z-z_{\mathrm{MI}})]\frac{\partial v(z,t)}{\partial t}=\left\langle\frac{\partial\sigma(z,t)}{\partial z}\right\rangle^{z}$$
$$[C^{-}H(z_{\mathrm{MI}}-z)+C^{+}H(z-z_{\mathrm{MI}})]\frac{\partial\sigma(z,t)}{\partial t}=\left\langle\frac{\partial v(z,t)}{\partial z}\right\rangle^{z}, \quad (16)$$

in which Heaviside unit step function is assumed as,

$$H(z)=0;z<0=\frac{1}{2};z=0=1;z>0. \quad (17)$$

Wavenumber-domain view

Spatially sampled terms. In a grid and in an FD scheme, all material parameters and field variables are individually spatially sampled. Instead of $\rho(z)$, $a(z,t)$, and $\sigma(z,t)$, consider functions spatially sampled using the shah (or Dirac comb) sampling function with period equal to the grid spacing h,

$$\delta_{(h)}(z):=\sum_{n=-\infty}^{\infty}\delta(z-nh)\ . \quad (18)$$

Fourier transform of the spatially sampled density is,

$$\mathcal{F}_{z\to k}\left\{\sum_{n=-\infty}^{\infty}\delta(z-nh)\rho(z)\right\}=\left[\frac{1}{h}\sum_{n=-\infty}^{\infty}\delta(k-n2k_N)\right]*^{k}\tilde{\rho}(k)=$$
$$=\frac{1}{h}\sum_{n=-\infty}^{\infty}\tilde{\rho}(k-n2k_N)=:\tilde{\rho}^{(2k_N)}(k). \quad (19)$$

Function $\tilde{\rho}^{(2k_N)}(k)$ is a $2k_N$-periodic repetition of the Fourier spectrum $\tilde{\rho}(k)$. Since $\tilde{\rho}(k)$ is nonzero in $[-\infty,\infty]$, $\tilde{\rho}^{(2k_N)}(k)$ is aliased in any interval $[k_0,k_0+2k_N]$, in which k_0 is an arbitrary real number. To avoid the aliasing, we must band-limit $\tilde{\rho}(k)$ in $[-k_N,k_N]$. Let us denote the band-limited function as $\tilde{\rho}_{k_N}(k)$ and its periodic repetition as $\tilde{\rho}_{k_N}^{(2k_N)}(k)$:

$$\frac{1}{h}\sum_{n=-\infty}^{\infty}\tilde{\rho}_{k_N}(k-n2k_N)=:\tilde{\rho}_{k_N}^{(2k_N)}(k). \quad (20)$$

Analogously, for the spatially sampled acceleration, we have,

$$\tilde{a}^{(2k_N)}(k):=\frac{1}{h}\sum_{n=-\infty}^{\infty}\tilde{a}(k-n2k_N), \quad (21)$$

and its band-limited version will be referred to as $\tilde{a}_{k_N}^{(2k_N)}(k)$. We recall that the wavefield function $\tilde{a}(k)$ is implicitly band limited (as explained in the Frequency–Wavenumber Domain View section). The spatially sampled stress is,

$$\tilde{\sigma}^{(2k_N)}(k):=\frac{1}{h}\sum_{n=-\infty}^{\infty}\tilde{\sigma}(k-n2k_N), \quad (22)$$

and its band-limited version is $\tilde{\sigma}_{k_N}^{(2k_N)}(k)$.

Equations with spatially sampled terms. Because equation (16) has the same structure, we can explicitly address only one of them. Consider the first of the equations. Omitting the symbol of averaging on the right side, we may write,

$$\rho(z)a(z,t)=\frac{\partial\sigma(z,t)}{\partial z}. \quad (23)$$

Consider a shah-sampling function applied to the equation:

$$\sum_{n=-\infty}^{\infty}\delta(z-nh)\rho(z)a(z,t)=\sum_{n=-\infty}^{\infty}\delta(z-nh)\frac{\partial\sigma(z,t)}{\partial z}. \quad (24)$$

Apply the Fourier transform to the left side of the preceding equation:

$$\mathcal{F}_{z\to k}\left\{\sum_{n=-\infty}^{\infty}\delta(z-nh)\rho(z)a(z,t)\right\}$$
$$=\mathcal{F}_{z\to k}\left\{\sum_{n=-\infty}^{\infty}\delta(z-nh)\rho(z)\right\}*^{k}\mathcal{F}_{z\to k}\{a(z,t)\}$$
$$=\tilde{\rho}^{(2k_N)}(k)*^{k}\tilde{a}(k). \quad (25)$$

Because $\tilde{a}(k)$ is band limited, the latter convolution can be written as a periodic convolution:

$$\tilde{\rho}^{(2k_N)}(k)*^{k,(2k_N)}\tilde{a}_{k_N}^{(2k_N)}(k):=\int_{-k_N}^{k_N}\tilde{\rho}^{(2k_N)}(k-k')\tilde{a}_{k_N}^{(2k_N)}(k')dk'. \quad (26)$$

To avoid aliasing of density, we have to replace $\tilde{\rho}^{(2k_N)}$ by its band-limited version:

$$\tilde{\rho}_{k_N}^{(2k_N)}(k)*^{k,\,(2k_N)}\tilde{a}_{k_N}^{(2k_N)}(k). \quad (27)$$

This is the periodic convolution of two $2k_N$-periodic functions in the wavenumber domain. The resulting convolution is therefore also a $2k_N$-periodic function. Since both $\tilde{\rho}_{k_N}(k)$ and $\tilde{a}_{k_N}(k)$ are $[-k_N,k_N]$ band-limited, the convolution is not aliased in $[-k_N,k_N]$.

We now transform the right side of equation (24) to the wavenumber domain:

$$\mathcal{F}_{z\to k}\left\{\sum_{n=-\infty}^{\infty}\delta(z-nh)\frac{\partial\sigma(z,t)}{\partial z}\right\}=\left[\frac{1}{h}\sum_{n=-\infty}^{\infty}\delta(k-n2k_N)\right]*^{k}ik\tilde{\sigma}(k,t). \quad (28)$$

Let us comment on term $ik\tilde{\sigma}(k,t)$. It is a Fourier transform of the spatial derivative of $\sigma(z,t)$: discontinuity of the spatial derivative at the material interface does not affect the Fourier-transform integral.

The right side of equation (28) is a $2k_N$-periodic repetition of $ik\tilde{\sigma}(k,t)$. Denote

$$\tilde{s}(k,t) := \tilde{d}(k)\tilde{\sigma}(k,t); \tilde{d}(k) := ik. \tag{29}$$

Then, the right side of equation (28) can be written as $\tilde{s}^{(2k_N)}(k,t)$. Function $\tilde{s}^{(2k_N)}(k,t)$ is a $2k_N$-periodic function. To avoid aliasing, function $\tilde{s}(k,t)$ must be band limited. As explained earlier, $\tilde{\sigma}(k,t)$ is implicitly band limited. We, however, must limit $\tilde{d}(k)$. We have already applied such limitation in the Frequency–Wavenumber Domain View section (equation 8). Denoting the band-limited $\tilde{d}(k)$ as $\tilde{d}_{k_N}(k)$, we can write a wavenumber version of equation (23) as,

$$\tilde{\rho}_{k_N}^{(2k_N)}(k) *^{k,(2k_N)} \tilde{a}_{k_N}^{(2k_N)}(k) = \tilde{d}_{k_N}^{(2k_N)}(k)\ \tilde{\sigma}_{k_N}^{(2k_N)}(k,t). \tag{30}$$

Return to the space domain. In this stage, we can apply an inverse Fourier transform to equation (30) to return to the space domain and our model of two half-spaces. Recall the density distribution:

$$\rho^- H(z_{\mathrm{MI}} - z) + \rho^+ H(z - z_{\mathrm{MI}}). \tag{31}$$

The Fourier transform in the wavenumber domain is,

$$\mathcal{F}_{z\to k}\{\rho(z)\} = \rho^-\left[\pi\delta(-k) + \frac{\exp(ikz_{\mathrm{MI}})}{ik}\right] + \rho^+\left[\pi\delta(k) - \frac{\exp(ikz_{\mathrm{MI}})}{ik}\right]. \tag{32}$$

The band-limited Fourier transform is,

$$\tilde{\rho}_{k_N}(k) = \tilde{w}(k)\left\{\rho^-[\pi\delta(-k) + \frac{\exp(ikz_{\mathrm{MI}})}{ik}\right] + \rho^+\left[\pi\delta(k) - \frac{\exp(ikz_{\mathrm{MI}})}{ik}\right]\Bigg\}, \tag{33}$$

with

$$\tilde{w}(k) = \Pi(k/k_N) = \begin{matrix} 1\ ; & k \in \langle -k_N, k_N\rangle \\ 0\ ; & k \notin \langle -k_N, k_N\rangle \end{matrix}. \tag{34}$$

The band-limited inverse Fourier transform of relation gives the band-limited density distribution in the space domain:

$$\rho_{k_N}(z) = \frac{1}{2}(\rho^- + \rho^+) + (\rho^+ - \rho^-)\frac{1}{\pi}\mathrm{Si}[k_N(z - z_{\mathrm{MI}})], \tag{35}$$

in which

$$\mathrm{Si}[k_N(z - z_{\mathrm{MI}})] := \int_0^{k_N(z-z_{\mathrm{MI}})} \frac{\sin u}{u}\,du. \tag{36}$$

Because the factors in equation (30) are $2k_N$ periodic, $\rho_{k_N}(z)$ must be spatially sampled in the space-domain equation: $\rho_{k_N}(z_n)$ with z_n representing discrete positions.

Eventually, equation (30) and an analogous one for the second of equation (16) are transformed to the following equations:

$$\left\{\frac{1}{2}(\rho^- + \rho^+) + (\rho^+ - \rho^-)\frac{1}{\pi}\mathrm{Si}[k_N(z_n - z_{\mathrm{MI}})]\right\}\frac{\partial v(z_n,t)}{\partial t} = \left[\frac{1}{h(z_n - z_{\mathrm{MI}})}\cos[k_N(z_n - z_{\mathrm{MI}})] - \frac{1}{\pi(z_n - z_{\mathrm{MI}})^2} \times \sin[k_N(z_n - z_{\mathrm{MI}})]\right] *^z \sigma(z_n,t)$$

$$\left\{\frac{1}{2}(C^- + C^+) + (C^+ - C^-)\frac{1}{\pi}\mathrm{Si}[k_N(z_n - z_{\mathrm{MI}})]\right\}\frac{\partial \sigma(z_n,t)}{\partial t} = \left[\frac{1}{h(z_n - z_{\mathrm{MI}})}\cos[k_N(z_n - z_{\mathrm{MI}})\right] - \frac{1}{\pi(z_n - z_{\mathrm{MI}})^2} \times \sin[k_N(z_n - z_{\mathrm{MI}})]\right] *^z v(z_n,t). \tag{37}$$

The spatial coordinate z_n indicates that the field variables and material parameters relate to discrete spatial positions equidistantly spaced with the grid spacing h.

Equation (37) is equation for spatially sampled field variables and material parameters. The equations, and thus the wave propagation in the spatial grid, are not affected by wavenumbers larger than k_N because in the wavenumber domain the functions are $2k_N$-periodic.

Figure 2 shows the band-limited distribution of the compliance in the second of equation (37). For comparison, the figure also shows a compliance corresponding to the band-limited shear modulus.

The second lesson from the wavenumber-domain view

Recall that equation (16) is valid for unlimited ranges of time, space, frequency, and wavenumber for the model of two homogeneous half-spaces. The spatial derivatives of the particle velocity and stress on the right sides of equation (16) are discontinuous at the material interface. Equation (37) is the $k \in \langle -k_N, k_N\rangle$ band-limited version of equation (16) for spatially sampled functions.

The discontinuous spatial derivatives at the material interface are replaced by continuous spatial convolutions. This means that the wavenumber band limitation removes discontinuities of the spatial derivatives of the particle velocity and stress at the material interface. Consequently, FD operators properly approximating the spatial convolutions can be applied across the material interface.

The heterogeneity of medium and the $k \in \langle -k_N, k_N\rangle$ band limitation of the equations have the important implication for an FD modeling: The grid representation of the heterogeneous

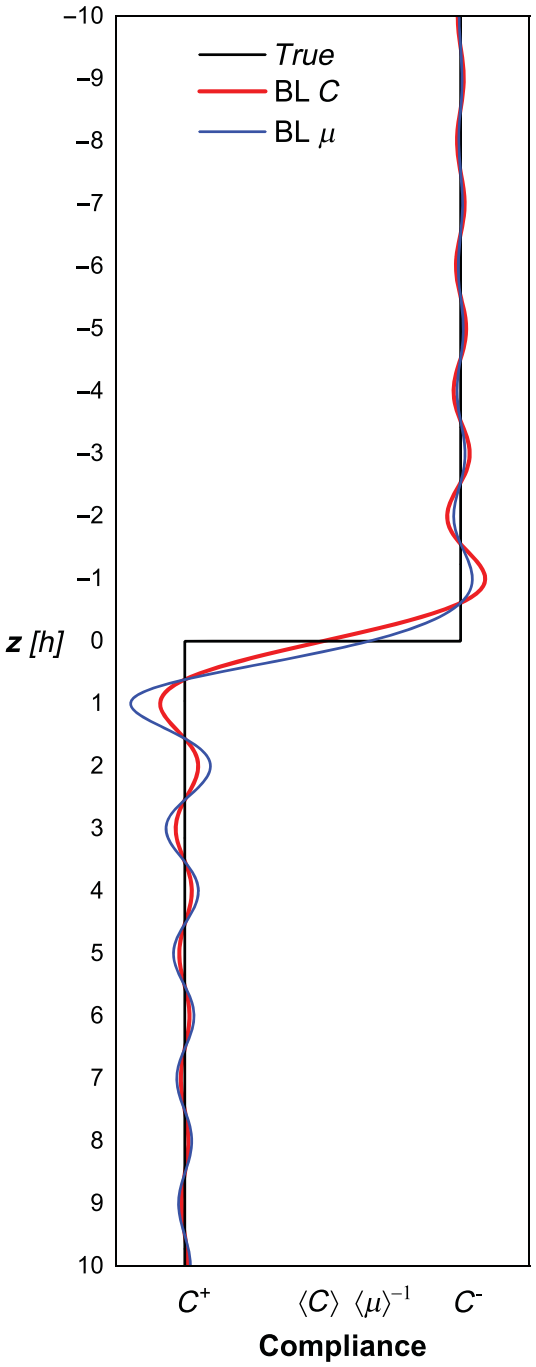

Figure 2. Illustration of the band-limited compliance distribution (BL C) and the true Heaviside distribution. A compliance corresponding to the band-limited shear modulus (BL μ) is also shown. It is obvious that the band-limited shear modulus does not give the same parameterization.

medium (generally heterogeneous, not necessarily only a medium with a single material interface) must be limited up to the Nyquist frequency k_N.

The other fundamental implication is that the material heterogeneity is represented only by the left sides of equation (13).

Consider another important aspect of the wavenumber-domain view: the wavenumber band limitation and its consequences are independent of choice of type of averaging: strictly mathematically, the arithmetic averaging is a reasonable but not an unambiguous choice. This also means that the value of the Heaviside function at $z = 0$ could remain undefined. However, the structure of the heterogeneous formulation (that is the structure of averaging) must be that in equation (13).

2D *SH* PROBLEM IN TWO HOMOGENEOUS HALF-SPACES

In this section, we consider a 2D *SH* problem which, in general, is described by the following V_S formulation:

$$\begin{aligned}\rho(z)\frac{\partial v(x,z,t)}{\partial t} &= \frac{\partial \sigma_{xy}(x,z,t)}{\partial x} + \frac{\partial \sigma_{yz}(x,z,t)}{\partial z}\\ C_\mu(z)\frac{\partial \sigma_{xy}(x,z,t)}{\partial t} &= \frac{\partial v(x,z,t)}{\partial x}\\ C_\mu(z)\frac{\partial \sigma_{yz}(x,z,t)}{\partial t} &= \frac{\partial v(x,z,t)}{\partial z}.\end{aligned} \tag{38}$$

Here, x and z are the horizontal and vertical coordinate axes, respectively, v is the particle velocity perpendicular to the vertical xz plane, σ_{xy} and σ_{yz} are shear stress components, ρ is density, and C_μ is compliance related to shear modulus μ as $C_\mu = 1/\mu$.

We consider the same model as in the 1D problem: two homogeneous half-spaces, labeled $-$ and $+$ for $z < z_{\mathrm{MI}}$ and $z > z_{\mathrm{MI}}$, respectively, with a welded material interface at $z = z_{\mathrm{MI}}$. Material parameters are discontinuous at the material interface.

The particle velocity v, stress component σ_{yz}, and spatial derivative $\partial v/\partial x$ are continuous at the material interface. The stress component σ_{xy}, and spatial derivatives $\partial v/\partial z$, $\partial \sigma_{xy}/\partial x$, and $\partial \sigma_{yz}/\partial z$ are discontinuous at the material interface.

Equations in the time–space domain

Velocity–stress equations inside half-spaces. With an obvious abbreviated notation, we may write the V_S equations in the half-spaces, omitting the independent variables for brevity, as,

$$\rho^- \frac{\partial v}{\partial t} = \frac{\partial \sigma_{xy}^-}{\partial x}\bigg|^- + \frac{\partial \sigma_{yz}}{\partial z}\bigg|^-, \rho^+ \frac{\partial v}{\partial t} = \frac{\partial \sigma_{xy}^+}{\partial x}\bigg|^+ + \frac{\partial \sigma_{yz}}{\partial z}\bigg|^+, \tag{39}$$

$$C_\mu^- \frac{\partial \sigma_{xy}^-}{\partial t} = \frac{\partial v}{\partial x}, C_\mu^+ \frac{\partial \sigma_{xy}^+}{\partial t} = \frac{\partial v}{\partial x} C_\mu^- \frac{\partial \sigma_{yz}}{\partial t} = \frac{\partial v}{\partial z}\bigg|^-, C_\mu^+ \frac{\partial \sigma_{yz}}{\partial t} = \frac{\partial v}{\partial z}\bigg|^+. \tag{40}$$

Velocity–stress equations at the material interface. In the equations of motion (equation 39), we arithmetically average discontinuous spatial derivatives of stress components at

the material interface. Consequently, also densities are arithmetically averaged at the material interface. In the constitutive relations for σ_{xy}, we arithmetically average temporal derivatives of σ_{xy}. Therefore, we obtain arithmetic averaging of shear moduli. In the constitutive relations for σ_{yz}, we arithmetically average spatial derivatives of v. Therefore, we obtain arithmetic averaging of compliances. Eventually, we obtain the following equations for the material interface:

$$\begin{aligned}\langle\rho\rangle^z\frac{\partial v}{\partial t}&=\left\langle\frac{\partial\sigma_{xy}}{\partial x}\right\rangle^z+\left\langle\frac{\partial\sigma_{yz}}{\partial z}\right\rangle^z\\ \frac{\partial}{\partial t}\langle\sigma_{xy}\rangle^z&=\langle\mu\rangle^z\frac{\partial v}{\partial x}\\ \langle C_\mu\rangle^z\frac{\partial\sigma_{yz}}{\partial t}&=\left\langle\frac{\partial v}{\partial z}\right\rangle^z.\end{aligned}\tag{41}$$

As we mentioned in the Elemental Consideration on a Material Interface in an FD Grid section, this is the proper structure of the heterogenous formulation consistent with principles explained by Backus (1962). Therefore, in view of the subsequent application of the Fourier transform to the wavenumber domain, we cannot use a formal alternative for the second equation in equation (41), that is, we cannot rewrite it as,

$$\langle C_\mu\rangle^{Hz}\frac{\partial\langle\sigma_{xy}\rangle^z}{\partial t}=\frac{\partial v}{\partial x},\tag{42}$$

in which

$$\langle C_\mu\rangle^{Hz}:=2\left(\frac{1}{C_\mu^-}+\frac{1}{C_\mu^+}\right)^{-1},\tag{43}$$

is the harmonic average of compliances. Equation (42) has a product of two discontinuous quantities on the lhs.

Velocity–stress equations for the entire model: A heterogeneous formulation. Equations can be also considered to be equations valid for the entire model—for the reasons explained in the 1D Problem in Two Homogeneous Half-Spaces section.

Importantly, equation (38) can be also considered to be a suitable and mathematically correct heterogeneous formulation for the entire model, if we properly define values of material parameters and spatial derivatives at the material interface.

Equation (41) can be specified for the entire model of the two homogeneous half-spaces:

$$\begin{aligned}[\rho^-H(-z)+\rho^+H(z)]\frac{\partial v}{\partial t}&=\left\langle\frac{\partial\sigma_{xy}}{\partial x}\right\rangle^z+\left\langle\frac{\partial\sigma_{yz}}{\partial z}\right\rangle^z\\ \frac{\partial\langle\sigma_{xy}\rangle^z}{\partial t}&=[\mu^-H(-z)+\mu^+H(z)]\frac{\partial v}{\partial x}\\ [C_\mu^-H(-z)+C_\mu^+H(z)]\frac{\partial\sigma_{yz}}{\partial t}&=\left\langle\frac{\partial v}{\partial z}\right\rangle^z.\end{aligned}\tag{44}$$

Wavenumber-domain view

Comparing equation (44) with (16), we see that we have a new type of term on the right side of the second of equation (44). Thus, we must address explicitly this term. For brevity, let us write it as,

$$\mu(z)\frac{\partial v(x,z,t)}{\partial x}.\tag{45}$$

Because the wavefield is 2D, we must apply sampling in both x and z directions.

An application of the Fourier transform $\mathcal{F}_{x\to k_x,z\to k_z}$ to the spatially sampled shear modulus gives,

$$\begin{aligned}&\left[\frac{1}{h}\sum_{m=-\infty}^{\infty}\delta(k_x-m2k_N)\right]\left\{\left[\frac{1}{h}\sum_{n=-\infty}^{\infty}\delta(k_z-n2k_N)\right]*^{k_z}\tilde{\mu}(k_z)\right\}\\ &:=\tilde{\mu}^{(2k_N,2k_N)}(k_x,k_z).\end{aligned}\tag{46}$$

Function $\tilde{\mu}^{(2k_N,2k_N)}(k_x,k_z)$ is a $2k_N$-periodic repetition of the Fourier spectrum $\tilde{\mu}(k_x,k_z)$ in both k_x and k_z. Since $\tilde{\mu}(k_z)$ is nonzero in the entire unlimited k_z range, $\tilde{\mu}^{(2k_N,2k_N)}(k_x,k_z)$ is aliased for $k_z\in[k_0,k_0+2k_N]$, in which k_0 is an arbitrary real number. To avoid the aliasing, we must band-limit $\tilde{\mu}(k_z)$ in $k_z\in[-k_N,k_N]$. Let us denote the band-limited function as $\tilde{\mu}_{k_N}(k_z)$ and the periodic repetition defined by as $\tilde{\mu}_{k_N}^{(2k_N,2k_N)}(k_x,k_z)$:

$$\begin{aligned}&\left[\frac{1}{h}\sum_{m=-\infty}^{\infty}\delta(k_x-m2k_N)\right]\left[\frac{1}{h}\sum_{n=-\infty}^{\infty}\tilde{\mu}_{k_N}(k_z-n2k_N)\right]\\ &:=\tilde{\mu}_{k_N}^{(2k_N,2k_N)}(k_x,k_z).\end{aligned}\tag{47}$$

An application of the Fourier transform $\mathcal{F}_{x\to k_x,z\to k_z}$ to the second factor in equation (45) with the spatially sampled particle velocity yields,

$$\begin{aligned}&\left\{\left[\frac{1}{h}\sum_{m=-\infty}^{\infty}\delta(k_x-m2k_N)\right]\left[\frac{1}{h}\sum_{n=-\infty}^{\infty}\delta(k_z-n2k_N)\right]\right\}\\ &*^{k_x,k_z}ik_x\tilde{v}(k_x,k_z,t).\end{aligned}\tag{48}$$

Let

$$\tilde{d}(k_x):=ik_x,\tag{49}$$

$$\tilde{q}(k_x,k_z,t):=\tilde{d}(k_x)\tilde{v}(k_x,k_z,t).\tag{50}$$

Equation (48) can be then written as $\tilde{q}^{(2k_N,2k_N)}(k_x,k_z,t)$. It is $2k_N$-periodic in both k_x and k_z. To avoid aliasing, $\tilde{q}(k_x,k_z,t)$ must be band limited. As already explained, we do not need to explicitly band limit $\tilde{v}(k_x,k_z,t)$. We, however, must limit $\tilde{d}(k_x)$—as in the Frequency–Wavenumber Domain View

section. Denoting the band-limited $\tilde{d}(k_x)$ as $\tilde{d}_{k_N}(k_x)$, we can write a wavenumber version of equation (45) as,

$$\tilde{\mu}_{k_N}^{(2k_N,2k_N)}(k_x,k_z) *^{k_z,(2k_N)} [\tilde{d}_{k_N}^{(2k_N)}(k_x)\tilde{v}_{k_N}^{(2k_N,2k_N)}(k_x,k_z,t)]. \quad (51)$$

This is the periodic convolution of two periodic functions analogous to convolution, as explained in the Wavenumber-Domain View section. The second equation of equation (44) can be then written as,

$$\frac{\partial\tilde{\sigma}_{xy,k_N}^{(2k_N,2k_N)}(k_x,k_z,t)}{\partial t} = \tilde{\mu}_{k_N}^{(2k_N,2k_N)}(k_x,k_z) *^{k_z,(2k_N)} [\tilde{d}_{k_N}^{(2k_N)}(k_x)\tilde{v}_{k_N}^{(2k_N,2k_N)}(k_x,k_z,t)]. \quad (52)$$

Return to the space domain. In this stage, we can apply an inverse Fourier transform to equation (44) to return to the space domain and our model of two half-spaces. Let $p \in \{\rho, \mu, C_\mu\}$ and

$$p(z) = p^- H(z_{\mathrm{MI}} - z) + p^+ H(z - z_{\mathrm{MI}}). \quad (53)$$

The Fourier transform in the wavenumber domain is,

$$\begin{aligned}\tilde{p}(k_x,k_z) &= \mathcal{F}_{x\to k_x, z\to k_z}\{p^- H(z_{\mathrm{MI}}-z)+p^+ H(z-z_{\mathrm{MI}})\}\\ &= \int_{-\infty}^{\infty}\int_{-\infty}^{\infty}[p^- H(z_{\mathrm{MI}}-z)+p^+ H(z-z_{\mathrm{MI}})]\exp[i(k_x x+k_z z)]dxdz\\ &= 2\pi\delta(k_x)\left\{p^-\left[\pi\delta(-k_z)+\frac{\exp(ik_z z_{\mathrm{MI}})}{ik_z}\right]\right.\\ &\left. + p^+\left[\pi\delta(k_z)-\frac{\exp(ik_z z_{\mathrm{MI}})}{ik_z}\right]\right\}. \end{aligned} \quad (54)$$

The band-limited Fourier transform is,

$$\tilde{p}_{k_N}(k_x,k_z) = \tilde{w}_{xz}(k_x,k_z)\tilde{p}(k_x,k_z), \quad (55)$$

in which

$$\tilde{w}_{xz}(k_x,k_z) = \begin{matrix}1; k_i \in \langle -k_N, k_N\rangle \\ 0; k_i \notin \langle -k_N, k_N\rangle\end{matrix}; i \in \{x,z\}. \quad (56)$$

The band-limited inverse Fourier transform of relation (equation 55) is,

$$p_{k_N}(x,z) = \frac{1}{2}(p^- + p^+) + (p^+ - p^-)\frac{1}{\pi}\mathrm{Si}[k_N(z - z_{\mathrm{MI}})]. \quad (57)$$

As explained in the Wavenumber-Domain View section, $p_{k_N}(x,z)$ must be spatially sampled in the space-domain equation: $p_{k_N}(x_m,z_n)$ with x_m and z_n representing discrete positions:

$$p_{k_N}(x_m,z_n) = \frac{1}{2}(p^- + p^+) + (p^+ - p^-)\frac{1}{\pi}\mathrm{Si}[k_N(z_n - z_{\mathrm{MI}})]. \quad (58)$$

Eventually, equation (44) is transformed to the following equation:

$$\begin{aligned}\rho_{k_N}(x_m,z_n)\frac{\partial v(x_m,z_n,t)}{\partial t} &= D_x(x_m) *^x \sigma_{xy}(x_m,z_n,t)\\ &+ D_z(z_n) *^z \sigma_{yz}(x_m,z_n,t)\\ \frac{\partial\sigma_{xy}(x_m,z_n,t)}{\partial t} &= \mu_{k_N}(x_m,z_n)[D_x(x_m) *^x v(x_m,z_n,t)]\\ C_{\mu k_N}(x_m,z_n)\frac{\partial\sigma_{yz}(x_m,z_n,t)}{\partial t} &= D_z(z_n) *^z v(x_m,z_n,t).\end{aligned} \quad (59)$$

Here,

$$\begin{aligned}D_x(x_m) &:= \frac{1}{\pi^2}\left[\frac{\pi}{h}\frac{1}{x_m}\cos(k_N x_m) - \frac{1}{x_m^2}\sin\left(\frac{\pi}{h}x_m\right)\right]D_z(z_n) :\\ &= \frac{1}{\pi^2}\left\{\frac{1}{h\Delta z_{n\mathrm{MI}}}\cos[k_N\Delta z_{n\mathrm{MI}}] - \frac{1}{\pi\Delta z_{n\mathrm{MI}}^2}\sin[k_N\Delta z_{n\mathrm{MI}}]\right\},\end{aligned} \quad (60)$$

in which

$$\Delta z_{n\mathrm{MI}} := z_n - z_{\mathrm{MI}}. \quad (61)$$

Equation (59) is equation for spatially sampled field variables and material parameters. The equations, and thus the wave propagation in the spatial grid, are not affected by wavenumbers larger than k_N because in the wavenumber domain the functions are $2k_N$-periodic and $\langle -k_N, k_N\rangle$ band limited. These equations are to be compared with equation (44).

The third lesson from the wavenumber-domain view

We have transformed the original equation (44) valid for unlimited ranges of time, space, frequency, and wavenumber to the $k_i \in \langle -k_N, k_N\rangle; i \in \{x,z\}$ band-limited equation (59) for spatially sampled functions.

In addition to the lesson formulated in The Second Lesson from the Wavenumber-Domain View section, the investigation of the 2D *SH* problem has brought another finding. The second and third of equation (59) are constitutive relations of an anisotropic medium. The true physical model for the 2D *SH* problem is isotropic, being described just by the shear modulus μ. It is clear from equation (41) that the averaging implies two material parameters needed for incorporating a simple horizontal planar interface between two homogeneous half-spaces: $\langle\mu\rangle^z$ and $\langle C_\mu\rangle^z$. The anisotropy of the effective wavenumber band-limited medium is illustrated in Figure 3 using Thomsen anisotropic parameter for the shear-wave speed ratios between the lower and upper half-spaces.

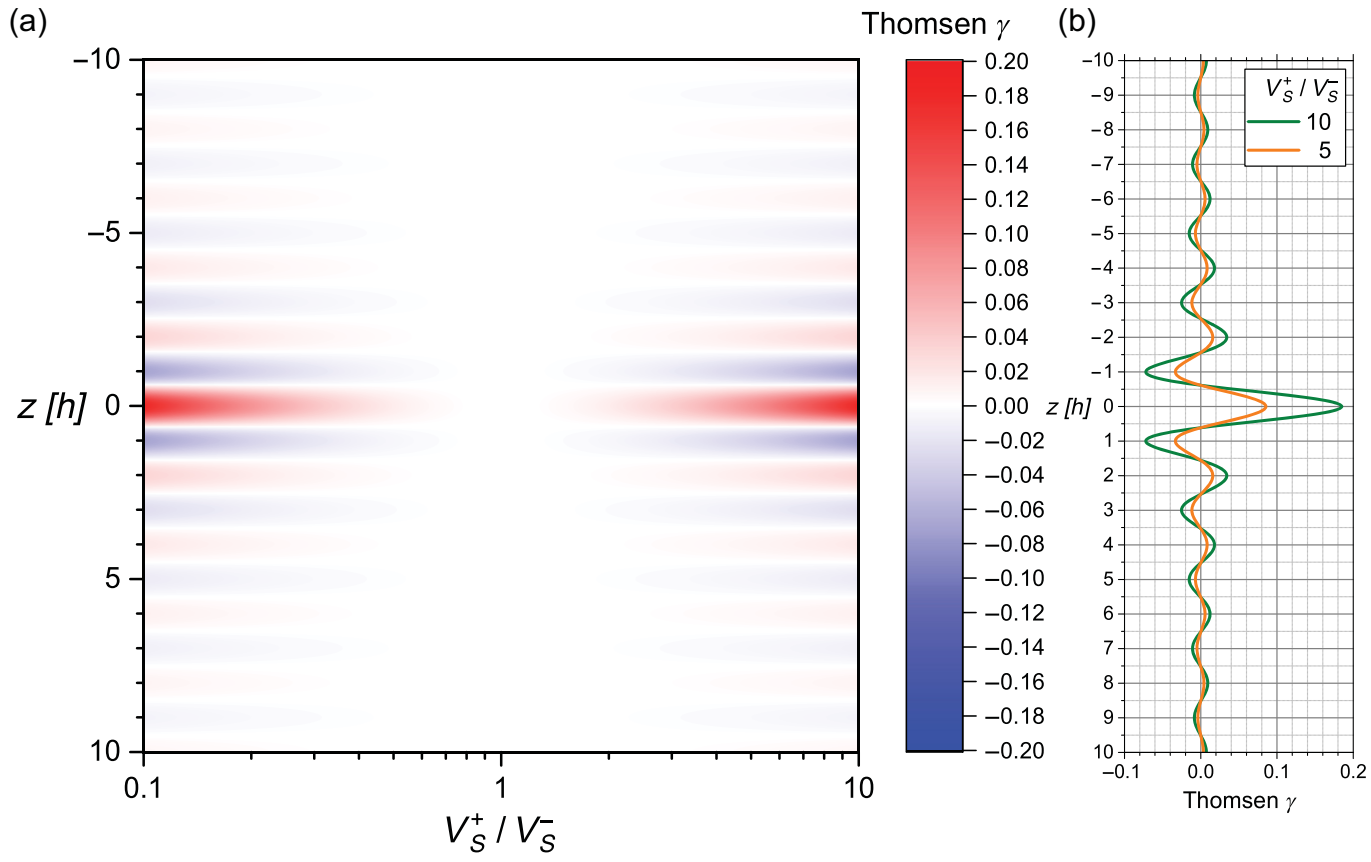

Is the latter consequence related to averaging or wavenumber band limitation? As explained in the Elemental Consideration on a Material Interface in an FD Grid section, these two aspects cannot be considered independent. Just opposite. The wavenumber limitation must be applied to the heterogeneous formulation which is determined by implementation of the boundary conditions and is consistent with principles of averaging (Backus, 1962). Both the heterogeneous formulation and wavenumber band limitation are the inevitable consequences of spatial discretization.

Let us add two comments related to the approaches by Mittet (2017) and Koene *et al.* (2022).

A dipping material interface in 2D *P–SV* problem is represented by Mittet (2017) using a 1D band-limited Heaviside function applied to compliance separately along grid lines in the one Cartesian direction and then in the other. Because Mittet (2017) applies the band-limited representation of the arithmetic averaging solely to the compliance, his approach is correct only in case of a plane wave propagating in the direction perpendicular to the material interface.

Koene *et al.* (2022) apply a 1D band-limited Heaviside function to compliance in the vertical Cartesian direction in case of the dipping interface. Therefore, their approach is correct only in case of a plane wave propagating in the vertical direction and horizontal material interface.

Figure 3. Illustration of anisotropy of the effective medium: Thomsen anisotropic parameter γ quantifying the level of anisotropy (a) for the range [0.1,10] of the shear-wave speed ratios between the lower and upper half-spaces and (b) for two values.

3D PROBLEM IN TWO HOMOGENEOUS HALF-SPACES

Equations in the time–space domain

Assuming all field variables being functions of spatial coordinates and time, and material parameters being functions of spatial coordinates, a 3D wavefield is described by equations of motion:

$$\rho \frac{\partial v_i}{\partial t} = \frac{\partial \sigma_{ij}}{\partial x_j}, i, j, k \in \{1, 2, 3\}, \tag{62}$$

and constitutive relations,

$$\frac{\partial \sigma_{ij}}{\partial t} = \lambda \frac{\partial \varepsilon_{kk}}{\partial t} \delta_{ij} + 2\mu \frac{\partial \varepsilon_{ij}}{\partial t}, \tag{63}$$

or, alternatively,

$$\frac{\partial \sigma_{ij}}{\partial t} = \lambda \frac{\partial v_k}{\partial x_k} \delta_{ij} + \mu \left(\frac{\partial v_i}{\partial x_j} + \frac{\partial v_j}{\partial x_i} \right), \tag{64}$$

since

$$\frac{\partial \varepsilon_{ij}}{\partial t} = \frac{1}{2}\left(\frac{\partial v_i}{\partial x_j} + \frac{\partial v_j}{\partial x_i}\right). \tag{65}$$

Here, λ is a Lamé parameter, ε_{ij} is the strain component, and δ_{ij} is Kronecker symbol. Other symbols have been already defined.

We consider the same model of two homogeneous half-spaces, labeled – and + for $z < z_{\mathrm{MI}}$ and $z > z_{\mathrm{MI}}$, respectively, with a welded material interface at $z = z_{\mathrm{MI}}$. Material parameters are discontinuous at the material interface.

Stress components $\sigma_{zx}, \sigma_{zy}, \sigma_{zz}$ and strain components $\varepsilon_{xx}, \varepsilon_{yy}, \varepsilon_{xy}$ are continuous at the material interface. Stress components $\sigma_{xx}, \sigma_{yy}, \sigma_{xy}$ and strain components $\varepsilon_{zx}, \varepsilon_{zy}, \varepsilon_{zz}$ are discontinuous at the material interface.

Equations inside half-spaces. We will omit here equations of motion for individual half-spaces because they are analogous to those in the 2D *SH* problem. In the following, we directly write equations for the material interface and the entire model. We must address, however, the constitutive relations. Inside half-spaces, we can write,

$$\begin{aligned} \sigma_{xx}^{-} &= M^{-}\varepsilon_{xx} + \lambda^{-}\varepsilon_{yy} + \lambda^{-}\varepsilon_{zz}^{-} \\ \sigma_{xx}^{+} &= M^{+}\varepsilon_{xx} + \lambda^{+}\varepsilon_{yy} + \lambda^{+}\varepsilon_{zz}^{+}, \end{aligned} \tag{66}$$

$$\begin{aligned} \sigma_{yy}^{-} &= \lambda^{-}\varepsilon_{xx} + M^{-}\varepsilon_{yy} + \lambda^{-}\varepsilon_{zz}^{-} \\ \sigma_{yy}^{+} &= \lambda^{+}\varepsilon_{xx} + M^{+}\varepsilon_{yy} + \lambda^{+}\varepsilon_{zz}^{+}, \end{aligned} \tag{67}$$

$$\begin{aligned} \sigma_{zz} &= \lambda^{-}\varepsilon_{xx} + \lambda^{-}\varepsilon_{yy} + M^{-}\varepsilon_{zz}^{-} \\ \sigma_{zz} &= \lambda^{+}\varepsilon_{xx} + \lambda^{+}\varepsilon_{yy} + M^{+}\varepsilon_{zz}^{+}, \end{aligned} \tag{68}$$

$$\begin{aligned} \sigma_{xy}^{-} &= 2\mu^{-}\varepsilon_{xy} \\ \sigma_{xy}^{+} &= 2\mu^{+}\varepsilon_{xy}, \end{aligned} \tag{69}$$

$$\begin{aligned} \sigma_{yz} &= 2\mu^{-}\varepsilon_{yz}^{-} \\ \sigma_{yz} &= 2\mu^{+}\varepsilon_{yz}^{+}, \end{aligned} \tag{70}$$

$$\sigma_{zx} = 2\mu^{-}\varepsilon_{zx}^{-}\sigma_{zx} = 2\mu^{+}\varepsilon_{zx}^{+}. \tag{71}$$

Stress components at the material interface. To account for the boundary conditions at the material interface, we arithmetically average discontinuous stress and strain components. Based on derivation in Appendix B, we obtain the following relations for the normal stress components at the material interface:

$$\begin{aligned} \langle \sigma_{xx} \rangle^{z} &= \langle \Theta \rangle^{z}\varepsilon_{xx} + \langle \mathrm{P} \rangle^{z}\varepsilon_{yy} + \langle \Gamma \rangle^{z}\sigma_{zz}\langle \sigma_{yy} \rangle^{z} \\ &= \langle \mathrm{P} \rangle^{z}\varepsilon_{xx} + \langle \Theta \rangle^{z}\varepsilon_{yy} + \langle \Gamma \rangle^{z}\sigma_{zz}\langle C_M \rangle^{z}\sigma_{zz} \\ &= \langle \Gamma \rangle^{z}\varepsilon_{xx} + \langle \Gamma \rangle^{z}\varepsilon_{yy} + \langle \varepsilon_{zz} \rangle^{z}. \end{aligned} \tag{72}$$

For the shear stress components, we easily obtain,

$$\langle \sigma_{xy} \rangle^{z} = 2\langle \mu \rangle^{z}\varepsilon_{xy}\langle C_\mu \rangle^{z}\sigma_{yz} = 2\langle \varepsilon_{yz} \rangle^{z}\langle C_\mu \rangle^{z}\sigma_{zx} = 2\langle \varepsilon_{zx} \rangle^{z}. \tag{73}$$

Coefficients are defined as,

$$\begin{aligned} &M := \lambda + 2\mu, \Gamma := \frac{\lambda}{M}, C_M := \frac{1}{M}, C_\mu := \frac{1}{\mu} \\ &\Theta := M - \lambda\Gamma = M - \frac{\lambda^2}{M}, \mathrm{P} := \lambda - \lambda\Gamma = \lambda - \frac{\lambda^2}{M}. \end{aligned} \tag{74}$$

Equations at the material interface and in the entire model. Similarly to the previous 1D and 2D problems, we can write equations valid at the material interface and also in the entire model in the velocity–stress formulation:

$$\begin{aligned} \langle \rho \rangle^{z}\frac{\partial v_x}{\partial t} &= \left\langle \frac{\partial \sigma_{xx}}{\partial x} \right\rangle^{z} + \left\langle \frac{\partial \sigma_{xy}}{\partial y} \right\rangle^{z} + \left\langle \frac{\partial \sigma_{xz}}{\partial z} \right\rangle^{z} \\ \langle \rho \rangle^{z}\frac{\partial v_y}{\partial t} &= \left\langle \frac{\partial \sigma_{yy}}{\partial y} \right\rangle^{z} + \left\langle \frac{\partial \sigma_{yz}}{\partial z} \right\rangle^{z} + \left\langle \frac{\partial \sigma_{yx}}{\partial x} \right\rangle^{z}, \\ \langle \rho \rangle^{z}\frac{\partial v_z}{\partial t} &= \left\langle \frac{\partial \sigma_{zz}}{\partial z} \right\rangle^{z} + \left\langle \frac{\partial \sigma_{zx}}{\partial x} \right\rangle^{z} + \left\langle \frac{\partial \sigma_{zy}}{\partial y} \right\rangle^{z} \end{aligned} \tag{75}$$

$$\begin{aligned} \frac{\partial}{\partial t}\langle \sigma_{xx} \rangle^{z} &= \langle \Theta \rangle^{z}\frac{\partial v_x}{\partial x} + \langle \mathrm{P} \rangle^{z}\frac{\partial v_y}{\partial y} + \langle \Gamma \rangle^{z}\frac{\partial \sigma_{zz}}{\partial t} \\ \frac{\partial}{\partial t}\langle \sigma_{yy} \rangle^{z} &= \langle \mathrm{P} \rangle^{z}\frac{\partial v_x}{\partial x} + \langle \Theta \rangle^{z}\frac{\partial v_y}{\partial y} + \langle \Gamma \rangle^{z}\frac{\partial \sigma_{zz}}{\partial t}, \\ \langle C_M \rangle^{z}\frac{\partial \sigma_{zz}}{\partial t} &= \langle \Gamma \rangle^{z}\frac{\partial v_x}{\partial x} + \langle \Gamma \rangle^{z}\frac{\partial v_y}{\partial y} + \left\langle \frac{\partial v_z}{\partial z} \right\rangle^{z} \end{aligned} \tag{76}$$

$$\begin{aligned} \left\langle \frac{\partial \sigma_{xy}}{\partial t} \right\rangle^{z} &= \langle \mu \rangle^{z}\left(\frac{\partial v_x}{\partial y} + \frac{\partial v_y}{\partial x}\right) \\ \langle C_\mu \rangle^{z}\frac{\partial \sigma_{yz}}{\partial t} &= \left\langle \frac{\partial v_y}{\partial z} + \frac{\partial v_z}{\partial y} \right\rangle^{z} \\ \langle C_\mu \rangle^{z}\frac{\partial \sigma_{zx}}{\partial t} &= \left\langle \frac{\partial v_z}{\partial x} + \frac{\partial v_x}{\partial z} \right\rangle^{z}. \end{aligned} \tag{77}$$

Let

$$p \in \{\rho, \mu, C_\mu, C_M, \Theta, \mathrm{P}, \Gamma\}. \tag{78}$$

Similarly to the previous 1D and 2D problems, we can specify equations (75)–(77) for the entire model of two half-spaces by considering the following expressions for the material parameters in the entire model:

$$\langle p \rangle^{z} = p^{-}H(z_{\mathrm{MI}} - z) + p^{+}H(z - z_{\mathrm{MI}}). \tag{79}$$

Transformed band-limited equations for spatially sampled functions

Comparing equations (44) and (75)–(77), we can see that the equations for the 3D problem do not include new type of term. This allows for generalizing the wavenumber-domain analysis in the 2D *SH* Problem in Two Homogeneous Half-Spaces section to the 3D problem and writing the transformed equations. Omitting discrete spatial positions and time as independent variables (x_m, y_j, z_n, t), we can write the equations in the following form:

$$\begin{aligned}\rho_{k_N}\frac{\partial v_x}{\partial t} &= D_x *^x \sigma_{xx} + D_y *^y \sigma_{xy} + D_z *^z \sigma_{xz}\rho_{k_N}\frac{\partial v_y}{\partial t}\\ &= D_y *^y \sigma_{yy} + D_z *^z \sigma_{yz} + D_x *^x \sigma_{yx}\rho_{k_N}\frac{\partial v_z}{\partial t}\\ &= D_z *^z \sigma_{zz} + D_x *^x \sigma_{zx} + D_y *^y \sigma_{zy},\end{aligned} \tag{80}$$

$$\begin{aligned}\frac{\partial \sigma_{xx}}{\partial t} &= \Theta_{k_N}[D_x *^x v_x] + \mathrm{P}_{k_N}[D_y *^y v_y] + \Gamma_{k_N}\frac{\partial \sigma_{zz}}{\partial t}\frac{\partial \sigma_{yy}}{\partial t}\\ &= \mathrm{P}_{k_N}[D_x *^x v_x] + \Theta_{k_N}[D_y *^y v_y] + \Gamma_{k_N}\frac{\partial \sigma_{zz}}{\partial t}C_{Mk_N}\frac{\partial \sigma_{zz}}{\partial t}\\ &= \Gamma_{k_N}[D_x *^x v_x] + \Gamma_{k_N}[D_y *^y v_y] + D_z *^z v_z,\end{aligned} \tag{81}$$

$$\begin{aligned}\frac{\partial \sigma_{xy}}{\partial t} &= \mu_{k_N}[D_y *^y v_x + D_x *^x v_y]\\ C_{\mu k_N}\frac{\partial \sigma_{yz}}{\partial t} &= D_z *^z v_y + D_y *^y v_z\\ C_{\mu k_N}\frac{\partial \sigma_{zx}}{\partial t} &= D_x *^x v_z + D_z *^z v_x,\end{aligned} \tag{82}$$

in which $D_x(x_m)$ and $D_z(z_n)$ are defined by equation (60):

$$D_y(y_j) := \frac{1}{\pi^2}\left[\frac{\pi}{h}\frac{1}{y_j}\cos(k_N y_j) - \frac{1}{y_j^2}\sin\left(\frac{\pi}{h}y_j\right)\right], \tag{83}$$

and p_{k_N} are defined by for p listed in.

The fourth lesson from the wavenumber-domain view

We have transformed the original equations (75)–(77) valid for unlimited ranges of time, space, frequency, and wavenumber to the $k_i \in \langle -k_N, k_N\rangle; i \in \{x, y, z\}$ band-limited equations (80)–(82) for spatially sampled functions. Compared to the previous 2D *SH* problem, the 3D wavefield in the same model of two homogeneous half-spaces does not provide substantial new insights related to the wavenumber band limitation.

It is interesting to rearrange constitutive relations to have temporal derivatives of the stress components on the left sides expressed solely using particle-velocity components on the right sides. This is done in Appendix C. The resulting stiffness matrix has elements that have structures similar to those in the stiffness matrix for the averaged medium in Kristek *et al.* (2017). The obtained effective medium is transversely isotropic in both cases. The substantial difference is in the wavenumber band limitation.

CONCLUSIONS

The main conclusions can be summarized as follows:

1. Based on the general elemental considerations and analysis of equations of motion and constitutive relations for four canonical model configurations, we demonstrated the following: if we want to solve, for example, velocity–stress equations by a heterogeneous FD scheme, we need (a) a heterogeneous formulation of the velocity–stress equations and (b) wavenumber band limitation. The heterogeneous formulation must be consistent with principles of averaging developed by Backus (1962). The wavenumber band limitation must be applied to the heterogeneous formulation.
2. We analyzed four canonical problems to identify the basic aspects of the FD discretization: 1D problem in an unbounded homogeneous medium, 1D problem in two homogeneous half-spaces, 2D *SH* problem in two homogeneous half-spaces, and 3D problem in two homogeneous half-spaces. Partial detailed findings and conclusions are formulated in the four sections on the lessons learned from the investigated problems.
3. In the four problems, we have found the Nyquist-wavenumber band-limited heterogeneous formulations of the velocity–stress equations. These are the equations that must be properly discretized by a heterogeneous FD scheme.
4. The wavenumber band limitation replaces spatial derivatives both in the homogeneous medium and across a material interface by continuous spatial convolutions. The latter means that the wavenumber band limitation removes discontinuities of the spatial derivatives of the particle velocity and stress at the material interface. This allows for applying proper FD operators across material interfaces.
5. The heterogeneity of the medium and the Nyquist-wavenumber (k_N) band limitation of the equations has the important implication for an FD modeling: The grid representation of the heterogeneous medium (generally heterogeneous, not necessarily only a medium with a single material interface) must be limited up to k_N.
6. The averaging and wavenumber band limitation imply anisotropy of the averaged medium already in the simple 2D *SH* problem of two homogeneous half-spaces with a material interface parallel with a coordinate plane (i.e., also with a grid plane).
7. In developing a heterogeneous FD scheme, the continuous spatial convolution of an infinite spatial extent must be properly replaced by a finite-extent discrete convolution.
8. The wavenumber band-limited spatial distribution representing a material interface has an infinite spatial extent

and a Gibbs phenomenon. Implementation in the FD scheme must properly solve both aspects.

9. A case of an oblique planar interface in an unbounded medium can be solved using rotation. A nonplanar interface in an unbounded medium as well as an interface (planar or nonplanar) in a model bounded by a free surface require separate studies accounting for the findings presented in this article.

DATA AND RESOURCES

No data are used in this study.

DECLARATION OF COMPETING INTERESTS

The authors acknowledge that there are no conflicts of interest recorded.

ACKNOWLEDGMENTS

This work was supported by the Slovak Research and Development Agency under the Contract APVV-15-0560 (project ID-EFFECTS) and by the Slovak Foxundation Grant VEGA 2/0046/20. The authors thank the reviewers for their constructive help. The authors are especially greatly indebted to Steven M. Day for his thoughtful criticism, discussion, and suggestions. The authors also thank Associate Editor Arben Pitarka and the Editor-in-Chief P. Martin Mai for their constructive help in improving this article.

REFERENCES

Backus, G. E. (1962). Long-wave elastic anisotropy produced by horizontal layering, *J. Geophys. Res.* **67,** 4427–4440.

Fichtner, A. (2011). *Full Seismic Waveform Modelling and Inversion*, Springer, Heidelberg, Germany.

Gregor, D., P. Moczo, J. Kristek, A. Mesgouez, G. Lefeuve-Mesgouez, and M. Kristekova (2021). Subcell-resolution finite-difference modelling of seismic waves in Biot and JKD poroelastic media, *Geophys. J. Int.* **224,** 760–794.

Gregor, D., P. Moczo, J. Kristek, A. Mesgouez, G. Lefeuve-Mesgouez, C. Morency, J. Diaz, and M. Kristekova (2022). Seismic waves in medium with poroelastic/elastic interfaces: A two-dimensional P-SV finite-difference modelling, *Geophys. J. Int.* **228,** 551–588.

Igel, H., P. Mora, and B. Riollet (1995). Anisotropic wave propagation through finite-difference grids, *Geophysics* **60,** 1203–1216.

Jiang, L., and W. Zhang (2021). TTI equivalent medium parametrization method for the seismic waveform modelling of heterogeneous media with coarse grids, *Geophys. J. Int.* **227,** 2016–2043.

Koene, E. F. M., J. Wittsten, and J. O. A. Robertsson (2022). Finite-difference modelling of 2-D wave propagation in the vicinity of dipping interfaces: A comparison of anti-aliasing and equivalent medium approaches, *Geophys. J. Int.* **229,** 70–96.

Kristek, J., P. Moczo, E. Chaljub, and M. Kristekova (2017). An orthorhombic representation of a heterogeneous medium for the finite-difference modelling of seismic wave propagation, *Geophys. J. Int.* **208,** 1250–1264.

Kristek, J., P. Moczo, E. Chaljub, and M. Kristekova (2019). A discrete representation of a heterogeneous viscoelastic medium for the finite-difference modelling of seismic wave propagation, *Geophys. J. Int.* **217,** 2021–2034.

Mittet, R. (2017). On the internal interfaces in finite-difference schemes, *Geophysics* **82,** T159–T182.

Mittet, R. (2021a). On the pseudospectral method and spectral accuracy, *Geophysics* **86,** T127–T142.

Mittet, R. (2021b). Small-scale medium variations with high-order finite-difference and pseudospectral schemes, *Geophysics* **86,** T387–T399.

Moczo, P. (1998). Introduction to modeling seismic wave propagation by the finite-difference method, *Lecture Notes*, Kyoto University, Japan, available at http://www.nuquake.eu/Publications/Moczo_LN_Kyoto_1998.pdf (last accessed November 2022).

Moczo, P., D. Gregor, J. Kristek, and J. de la Puente (2019). A discrete representation of material heterogeneity for the finite-difference modelling of seismic wave propagation in a poroelastic medium, *Geophys. J. Int.* **216,** 1072–1099.

Moczo, P., J. Kristek, P.-Y. Bard, S. Stripajová, F. Hollender, Z. Chovanová, M. Kristeková, and D. Sicilia (2018). Key structural parameters affecting earthquake ground motion in 2D and 3D sedimentary structures, *Bull. Earthq. Eng.* **16,** 2421–2450.

Moczo, P., J. Kristek, A.-A. Gabriel, E. Chaljub, J.-P. Ampuero, F.-J. Sánchez-Sesma, M. Galis, D. Gregor, and M. Kristekova (2021). Numerical wave propagation simulation, in *ESG 2021, The 6th IASPEI/IAEE International Symposium: Effects of Surface Geology on Seismic Motion*,H. Kawase, S. Hagashi, S. Tsuno, and H. Sato (Editors), 30 August–01 September 2021, Kyoto, Japan, (USB, paper ID: GS3-I03), available at http://www.nuquake.eu/Publications/Moczo_etal_ESG2021.pdf (last accessed November 2022).

Moczo, P., J. Kristek, and M. Galis (2014). *The Finite-Difference Modelling of Earthquake Motions: Waves and Ruptures*, Cambridge University Press, Cambridge, England.

Mora, P. (1986). Elastic finite differences with convolutional operators, *Stanford Explor. Proj. Rep.* **48,** 277–289.

Muir, F., J. Dellinger, J. Etgen, and D. Nichols (1992). Modeling elastic fields across irregular boundaries, *Geophysics* **57,** 1189–1193.

Schoenberg, M., and F. Muir (1989). A calculus for finely layered anisotropic media, *Geophysics* **54,** 581–589.

Vishnevsky, D., V. Lisitsa, V. Tcheverda, and G. Reshetova (2014). Numerical study of the interface errors of finite-difference simulations of seismic waves, *Geophysics* **79,** T219–T232.

Zahradník, J., and E. Priolo (1995). Heterogeneous formulation of elastodynamic equations and finite-difference schemes, *Geophys. J. Int.* **120,** 663–676.

Zhou, H., Y. Liu, and J. Wang (2021). Elastic wave modeling with high-order temporal and spatial accuracies by a selectively modified and linearly optimized staggered-grid finite-difference scheme, *IEEE Trans. Geosci. Remote Sens.* **60,** 1–22.

APPENDIX A

Band-limited inverse Fourier transform of a spectral product

Let,

$$\tilde{\varphi}_j(k) = \mathcal{F}_{z\to k}\{\varphi_j(z)\} \equiv \int_{-\infty}^{\infty} \varphi_j(z)\exp(ikz)dz$$

$$\varphi_j(z) = \mathcal{F}^{-1}_{k\to z}\{\tilde{\varphi}_j(k)\} \equiv \frac{1}{2\pi}\int_{-\infty}^{\infty} \tilde{\varphi}_j(k)\exp(-ikz)\,dk \;;\; j\in\{1,2\}. \tag{A1}$$

The inverse Fourier transform of the spectral product is,

$$\mathcal{F}^{-1}_{k\to z}\{\tilde{\varphi}_1(k)\tilde{\varphi}_2(k)\} \equiv \mathcal{F}^{-1}_{k\to z}|^{\infty}_{-\infty}\{\tilde{\varphi}_1(k)\tilde{\varphi}_2(k)\}. \tag{A2}$$

If the spectral product $\tilde{\varphi}_1(k)\tilde{\varphi}_2(k)$ is equal to zero outside $\langle -k_{\max}, k_{\max}\rangle$, the integration over $(-\infty, \infty)$ can be replaced by integration over $\langle -k_{\max}, k_{\max}\rangle$:

$$\begin{aligned}\mathcal{F}^{-1}_{k\to z}|^{\infty}_{-\infty}\{\tilde{\varphi}_1(k)\tilde{\varphi}_2(k)\} &= \mathcal{F}^{-1}_{k\to z}|^{k_{\max}}_{-k_{\max}}\{\tilde{\varphi}_1(k)\tilde{\varphi}_2(k)\}\\ &= \frac{1}{2\pi}\int_{-k_{\max}}^{k_{\max}}\int_{-\infty}^{\infty}\varphi_1(\tau)\exp(ik\tau)d\tau\\ &\times\int_{-\infty}^{\infty}\varphi_2(\vartheta)\exp(ik\vartheta)d\vartheta\exp(-ikz)dk.\end{aligned} \tag{A3}$$

Consider now the convolution,

$$\varphi(z) \equiv \varphi_1(z) *^z \varphi_2(z) = \int_{-\infty}^{\infty}\varphi_1(\tau)\varphi_2(z-\tau)d\tau, \tag{A4}$$

and the convolution theorem,

$$\mathcal{F}_{z\to k}\{\varphi(z)\} \equiv \mathcal{F}_{z\to k}\{\varphi_1(z) *^z \varphi_2(z)\} = \tilde{\varphi}_1(k)\tilde{\varphi}_2(k) = \tilde{\varphi}(k). \tag{A5}$$

At the same time, obviously,

$$\varphi(z) = \frac{1}{2\pi}\int_{-\infty}^{\infty}\tilde{\varphi}(k)\exp(-ikz)dk. \tag{A6}$$

Then,

$$\begin{aligned}\varphi(z) &= \varphi_1(z) *^z \varphi_1(z)\\ &= \frac{1}{2\pi}\int_{-\infty}^{\infty}\tilde{\varphi}(k)\exp(-ikz)dk = \frac{1}{2\pi}\int_{-\infty}^{\infty}\tilde{\varphi}_1(k)\tilde{\varphi}_2(k)\exp(-ikz)dk\\ &= \frac{1}{2\pi}\int_{-\infty}^{\infty}\int_{-\infty}^{\infty}\varphi_1(\vartheta)\exp(ik\vartheta)d\vartheta\int_{-\infty}^{\infty}\varphi_2(\theta)\exp(ik\theta)d\theta\exp(-ikz)dk.\end{aligned} \tag{A7}$$

Recalling that $\tilde{\varphi}_1(k)\tilde{\varphi}_2(k)$ is equal to zero outside $\langle -k_{\max}, k_{\max}\rangle$,

$$\begin{aligned}\varphi_1(z) *^z \varphi_2(z) &= \frac{1}{2\pi}\int_{-k_{\max}}^{k_{\max}}\int_{-\infty}^{\infty}\varphi_1(\vartheta)\exp(ik\vartheta)d\vartheta\\ &\times\int_{-\infty}^{\infty}\varphi_2(\theta)\exp(ik\theta)d\theta\exp(-ikz)dk.\end{aligned} \tag{A8}$$

We know that,

$$\varphi_1(z) *^z \varphi_2(z) = \mathcal{F}^{-1}_{k\to z}\{\tilde{\varphi}_1(k)\} *^z \mathcal{F}^{-1}_{k\to z}\{\tilde{\varphi}_2(k)\}. \tag{A9}$$

If we now assume that each of $\tilde{\varphi}_1(k)$ and $\tilde{\varphi}_2(k)$ is equal to zero outside $\langle -k_{\max}, k_{\max}\rangle$, we have,

$$\begin{aligned}\varphi_1(z) *^z \varphi_2(z) &= \mathcal{F}^{-1}_{k\to z}\{\tilde{\varphi}_1(k)\} *^z \mathcal{F}^{-1}_{k\to z}\{\tilde{\varphi}_2(k)\}\\ &= \mathcal{F}^{-1}_{k\to z}|^{k_{\max}}_{-k_{\max}}\{\tilde{\varphi}_1(k)\} *^z \mathcal{F}^{-1}_{k\to z}|^{k_{\max}}_{-k_{\max}}\{\tilde{\varphi}_2(k)\}.\end{aligned} \tag{A10}$$

Comparing equations (A3), (A8), and (A10), we obtain,

$$\begin{aligned}&\mathcal{F}^{-1}_{k\to z}|^{k_{\max}}_{-k_{\max}}\{\tilde{\varphi}_1(k)\tilde{\varphi}_2(k)\}\\ &= \mathcal{F}^{-1}_{k\to z}|^{k_{\max}}_{-k_{\max}}\{\tilde{\varphi}_1(k)\} *^z \mathcal{F}^{-1}_{k\to z}|^{k_{\max}}_{-k_{\max}}\{\tilde{\varphi}_2(k)\},\end{aligned} \tag{A11}$$

for $\tilde{\varphi}_1(k)$ and $\tilde{\varphi}_2(k)$ equal to zero outside $\langle -k_{\max}, k_{\max}\rangle$.

APPENDIX B
Averaging procedure applied to normal stress components

Consider first the continuous stress component σ_{zz}. With an obvious abbreviated notation, we may write for the two half-spaces:

$$\begin{aligned}\frac{1}{M^-}\sigma_{zz} &= \frac{\lambda^-}{M^-}\varepsilon_{xx} + \frac{\lambda^-}{M^-}\varepsilon_{yy} + \varepsilon^-_{zz}\\ \frac{1}{M^+}\sigma_{zz} &= \frac{\lambda^+}{M^+}\varepsilon_{xx} + \frac{\lambda^+}{M^+}\varepsilon_{yy} + \varepsilon^+_{zz}.\end{aligned} \tag{B1}$$

Let,

$$\Gamma \equiv \frac{\lambda}{M}, \quad C_M \equiv \frac{1}{M}. \tag{B2}$$

Then,

$$C^-_M\sigma_{zz} = \Gamma^-\varepsilon_{xx} + \Gamma^-\varepsilon_{yy} + \varepsilon^-_{zz}C^+_M\sigma_{zz} = \Gamma^+\varepsilon_{xx} + \Gamma^+\varepsilon_{yy} + \varepsilon^+_{zz}. \tag{B3}$$

Averaging the two equations, we obtain,

$$\langle C_M\rangle^z\sigma_{zz} = \langle\Gamma\rangle^z\varepsilon_{xx} + \langle\Gamma\rangle^z\varepsilon_{yy} + \langle\varepsilon_{zz}\rangle^z. \tag{B4}$$

Continue with σ_{xx} for which we may write,

$$\sigma^-_{xx} = M^-\varepsilon_{xx} + \lambda^-\varepsilon_{yy} + \lambda^-\varepsilon^-_{zz}\sigma^+_{xx} = M^+\varepsilon_{xx} + \lambda^+\varepsilon_{yy} + \lambda^+\varepsilon^+_{zz}. \tag{B5}$$

We need to express ε^-_{zz} and ε^+_{zz} using continuous field variables. From equation (B3), we have,

$$\varepsilon^-_{zz} = -\Gamma^-\varepsilon_{xx} - \Gamma^-\varepsilon_{yy} + C^-_M\sigma_{zz}\varepsilon^+_{zz} = -\Gamma^+\varepsilon_{xx} - \Gamma^+\varepsilon_{yy} + C^+_M\sigma_{zz}. \tag{B6}$$

Substitute ε_{zz}^{-} and ε_{zz}^{+} in equation (B5) by the right sides of equation (B6):

$$\sigma_{xx}^{-} = M^{-}\varepsilon_{xx} + \lambda^{-}\varepsilon_{yy} - \lambda^{-}\Gamma^{-}\varepsilon_{xx} - \lambda^{-}\Gamma^{-}\varepsilon_{yy} + \lambda^{-}C_M^{-}\sigma_{zz}$$
$$\sigma_{xx}^{+} = M^{+}\varepsilon_{xx} + \lambda^{+}\varepsilon_{yy} - \lambda^{+}\Gamma^{+}\varepsilon_{xx} - \lambda^{+}\Gamma^{+}\varepsilon_{yy} + \lambda^{+}C_M^{+}\sigma_{zz}. \quad \text{(B7)}$$

Considering,

$$\lambda C_M = \lambda/M = \Gamma, \Theta \equiv M - \lambda\Gamma, \mathrm{P} \equiv \lambda - \lambda\Gamma, \quad \text{(B8)}$$

we obtain,

$$\sigma_{xx}^{-} = \Theta^{-}\varepsilon_{xx} + \mathrm{P}^{-}\varepsilon_{yy} + \Gamma^{-}\sigma_{zz}$$
$$\sigma_{xx}^{+} = \Theta^{+}\varepsilon_{xx} + \mathrm{P}^{+}\varepsilon_{yy} + \Gamma^{+}\sigma_{zz}. \quad \text{(B9)}$$

Averaging the two equations, we have,

$$\langle\sigma_{xx}\rangle^{z} = \langle\Theta\rangle^{z}\varepsilon_{xx} + \langle\mathrm{P}\rangle^{z}\varepsilon_{yy} + \langle\Gamma\rangle^{z}\sigma_{zz}. \quad \text{(B10)}$$

Eventually, consider σ_{yy}:

$$\sigma_{yy}^{-} = \lambda^{-}\varepsilon_{xx} + M^{-}\varepsilon_{yy} + \lambda^{-}\varepsilon_{zz}^{-}\sigma_{yy}^{+} = \lambda^{+}\varepsilon_{xx} + M^{+}\varepsilon_{yy} + \lambda^{+}\varepsilon_{zz}^{+}. \quad \text{(B11)}$$

Substitute ε_{zz}^{-} and ε_{zz}^{+} in equation (B11) by the right sides of equation (B6):

$$\sigma_{yy}^{-} = \lambda^{-}\varepsilon_{xx} + M^{-}\varepsilon_{yy} - \lambda^{-}\Gamma^{-}\varepsilon_{xx} - \lambda^{-}\Gamma^{-}\varepsilon_{yy} + \lambda^{-}C_M^{-}\sigma_{zz}$$
$$\sigma_{yy}^{+} = \lambda^{+}\varepsilon_{xx} + M^{+}\varepsilon_{yy} - \lambda^{+}\Gamma^{+}\varepsilon_{xx} - \lambda^{+}\Gamma^{+}\varepsilon_{yy} + \lambda^{+}C_M^{+}\sigma_{zz}. \quad \text{(B12)}$$

After an easy rearrangement, we obtain,

$$\sigma_{yy}^{-} = \mathrm{P}^{-}\varepsilon_{xx} + \Theta^{-}\varepsilon_{yy} + \Gamma^{-}\sigma_{zz}\sigma_{yy}^{+} = \mathrm{P}^{+}\varepsilon_{xx} + \Theta^{+}\varepsilon_{yy} + \Gamma^{+}\sigma_{zz}, \quad \text{(B13)}$$

and after averaging the two latter equations, we have,

$$\langle\sigma_{yy}\rangle^{z} = \langle\mathrm{P}\rangle^{z}\varepsilon_{xx} + \langle\Theta\rangle^{z}\varepsilon_{yy} + \langle\Gamma\rangle^{z}\sigma_{zz}. \quad \text{(B14)}$$

APPENDIX C
Rearrangement of the wavenumber band-limited equations in the 3D problem of two homogeneous half-spaces

Rearrange constitutive relations equations (81) and (82) to have temporal derivatives of stress components on the left sides expressed solely using particle-velocity components on the right sides:

$$\begin{aligned}\frac{\partial\sigma_{xx}}{\partial t} &= \left[\Theta_{k_N} + \frac{(\Gamma_{k_N})^2}{C_{Mk_N}}\right][D_x *^{x} v_x] + \left[\mathrm{P}_{k_N} + \frac{(\Gamma_{k_N})^2}{C_{Mk_N}}\right][D_y *^{y} v_y] \\ &\quad + \frac{\Gamma_{k_N}}{C_{Mk_N}}[D_z *^{z} v_z]\frac{\partial\sigma_{xx}}{\partial t} \\ &= \left[\mathrm{P}_{k_N} + \frac{(\Gamma_{k_N})^2}{C_{Mk_N}}\right][D_x *^{x} v_x] + \left[\Theta_{k_N} + \frac{(\Gamma_{k_N})^2}{C_{Mk_N}}\right][D_y *^{y} v_y] \\ &\quad + \frac{\Gamma_{k_N}}{C_{Mk_N}}[D_z *^{z} v_z]\frac{\partial\sigma_{zz}}{\partial t} \\ &= \frac{\Gamma_{k_N}}{C_{Mk_N}}[D_x *^{x} v_x] + \frac{\Gamma_{k_N}}{C_{Mk_N}}[D_y *^{y} v_y] + \frac{1}{C_{Mk_N}}[D_z *^{z} v_z],\end{aligned} \quad \text{(C1)}$$

$$\frac{\partial\sigma_{xy}}{\partial t} = \mu_{k_N}[D_y *^{y} v_x + D_x *^{x} v_y]$$
$$\frac{\partial\sigma_{yz}}{\partial t} = \frac{1}{C_{\mu k_N}}[D_z *^{z} v_y + D_y *^{y} v_z]$$
$$\frac{\partial\sigma_{zx}}{\partial t} = \frac{1}{C_{\mu k_N}}[D_x *^{x} v_z + D_z *^{z} v_x]. \quad \text{(C2)}$$

Denote

$$\frac{\partial\vec{\sigma}}{\partial t} \equiv \left[\frac{\partial\sigma_{xx}}{\partial t}, \frac{\partial\sigma_{yy}}{\partial t}, \frac{\partial\sigma_{zz}}{\partial t}, \frac{\partial\sigma_{xy}}{\partial t}, \frac{\partial\sigma_{yz}}{\partial t}, \frac{\partial\sigma_{zx}}{\partial t}\right]^{T}$$
$$\frac{\partial\vec{\varepsilon}}{\partial t} \equiv \left[\frac{\partial v_x}{\partial x}, \frac{\partial v_y}{\partial y}, \frac{\partial v_z}{\partial z}, \frac{\partial v_x}{\partial y} + \frac{\partial v_y}{\partial x}, \frac{\partial v_y}{\partial z} + \frac{\partial v_z}{\partial y}, \frac{\partial v_z}{\partial x} + \frac{\partial v_x}{\partial z}\right]^{T}, \quad \text{(C3)}$$

and

$$\begin{aligned}A_{k_N} &\equiv \frac{1}{\left[\frac{1}{M}\right]_{k_N}}, B_{k_N} \equiv \frac{1}{\left[\frac{1}{M}\right]_{k_N}}\left[\frac{\lambda}{M}\right]_{k_N} C_{k_N} \equiv \Theta_{k_N} + \frac{(\Gamma_{k_N})^2}{C_{Mk_N}} \\ &= \left[M - \frac{\lambda^2}{M}\right]_{k_N} + \left\{\left[\frac{\lambda}{M}\right]_{k_N}\right\}^2 \frac{1}{\left[\frac{1}{M}\right]_{k_N}} D_{k_N} \equiv \mathrm{P}_{k_N} + \frac{(\Gamma_{k_N})^2}{C_{Mk_N}} \\ &= \left[\lambda - \frac{\lambda^2}{M}\right]_{k_N} + \left\{\left[\frac{\lambda}{M}\right]_{k_N}\right\}^2 \frac{1}{\left[\frac{1}{M}\right]_{k_N}}.\end{aligned} \quad \text{(C4)}$$

Then, the wavenumber $k \in \langle -k_N, k_N\rangle$ band-limited constitutive relations can be written as,

$$\frac{\partial\vec{\sigma}}{\partial t}|_{k_N} = \mathbf{E}_{k_N}\frac{\partial\vec{\varepsilon}}{\partial t}|_{k_N}, \quad \text{(C5)}$$

$$\mathbf{E}_{k_N} \equiv \begin{bmatrix} C_{k_N} & D_{k_N} & B_{k_N} & 0 & 0 & 0 \\ D_{k_N} & C_{k_N} & B_{k_N} & 0 & 0 & 0 \\ B_{k_N} & B_{k_N} & A_{k_N} & 0 & 0 & 0 \\ 0 & 0 & 0 & \mu_{k_N} & 0 & 0 \\ 0 & 0 & 0 & 0 & \frac{1}{C_{\mu k_N}} & 0 \\ 0 & 0 & 0 & 0 & 0 & \frac{1}{C_{\mu k_N}} \end{bmatrix}. \quad \text{(C6)}$$

Compare this with the corresponding matrix in Kristek *et al.* (2017). The matrix elements resemble elements of the stiffness matrix for the averaged medium in Kristek *et al.* (2017). The substantial difference is in the wavenumber band limitation.

Manuscript received 6 July 2022
Published online 17 November 2022